Various Factors and Propagation Trends of Stress Waves in Cross Sections of Euphrates Poplar

Shanqing Liang
Feng Fu
Lanying Lin
Nana Hu

Abstract

Various factors and propagation trends of stress waves in cross sections of wood need study to improve accuracy in the quality evaluation of wood and decay detection in standing trees. In this study, a Fakopp Microsecond Timer was used to measure the stress wave transmission time of Euphrates poplar (*Populus euphratica* Oliv.). Velocity was calculated to find the trend and make wavefront maps of stress waves. Results indicated that stress waves travel fastest in the radial direction and that velocity decreased as the angle between the two sensors increased. Velocity also increased as the number of annual rings increased. At the same time, the velocity in normal wood was higher than it was in tension wood, and it gradually increased in normal wood as the radial distance increased from pith to bark. Different influences on the stress wave propagation in wood were found when holes were made in the center of a cross section. Velocity showed little change with the increase in hole diameter when the angle between impacting and receiving sensors was 90°. At 180°, velocity was affected by hole diameter and rapidly decreased. Successful simulated wavefront maps of stress waves in cross sections of sound, hole, crack, and decay wood using two-dimensional contours were made. Three-dimensional maps were also reconstructed using Kriging interpolation and showed high similarity between cross sections.

Assessing wood quality of trees using acoustic methods is affected by anisotropy of wood, which leads to a complex propagation process of waves controlled by the fiber properties, fiber orientation, and fiber microstructure (Wang et al. 2005a). Strong relationships between transmission time, wave natural frequency, vibration amplitude, and wood properties can be used to effectively predict the mechanical properties of wood. Compared with other parameters, however, the transmission time, or wave velocity, is better explained and converted with an equation to evaluate the wood properties (Pellerin et al. 1986). In general, a stress wave can pass transversely through a timber in three different ways: The wave can go perpendicular to the rings, parallel to the rings, or cross the rings at an angle between 0° and 90° (Ross et al. 1999). Investigators have observed that the velocity of a stress wave varies with the direction in which a sound wave is transmitted through a stem and that velocity is the highest in the radial direction (Liang et al. 2008). However, the stress wave velocity is affected when defects are present in wood so that velocity in the tangential direction has higher values than velocity in the radial direction, especially when severe decay and hollow areas appear in the center of a stem.

Some studies have investigated the feasibility of using stress waves in the radial direction to evaluate stem defects (Ross et al. 1994, Schad et al. 1996, Yamamoto et al. 1998, Wang et al. 2004). More accurate inspection methods have also been developed to locate defects with a stress wave tomogram using multiple sensors (Divos and Sazlai 2002, Schwarze et al. 2004, Grabianowski et al. 2006, Wang et al. 2009). To accurately find or locate defects in wood, longitudinal stress waves (P-waves) propagating in the cross section of a log or tree trunk need to be studied and analyzed (Nicolotti et al. 2003, Gilbert and Smiley 2004,

The authors are, respectively, Associate Profession, Project Leader, Associate Profession, and PhD Candidate, Research Inst. of Wood Industry, Chinese Academy of Forestry, Beijing, China (liangsq@caf.ac.cn, feng@caf.ac.cn, linly@caf.ac.cn, hunana@caf.ac.cn). This paper was received for publication in September 2009. Article no. 10681.

Forest Prod. J. 60(5):440–446.

Larsson et al. 2004). So far, several types of equipment, including the Fakopp Microsecond Timer and the Arbotom and Picus Sonic Tomographs, have been used to inspect wood for defects that might affect velocity change or tomogram presentation (Divos and Divos 2005, Wang et al. 2005b, Wang et al. 2007). This equipment needs to be understood regarding the propagating path of stress waves and the variation in velocity under different test conditions, including number of sensors, angle between two sensors, and defect type and dimension. Therefore, knowledge regarding the propagating trend and various factors of stress waves in a cross section of a stem is important for improving tomograms and the evaluation of defects.

The objective of the present study was to investigate the propagating trend and various factors of stress waves in cross sections of wood as well as the relationship between hole diameter, angle between two sensors, tree age, normal wood and tension wood, radial distance from pith to bark, and transmission time and velocity of sound waves. A particularly important aim was to record the stress wave propagation path using two-dimensional and three-dimensional (3D) maps.

Materials and Methods

To investigate transmission path variation of a stress wave in a cross section of wood, three Euphrates poplar (*Populus euphratica* Oliv.) trees from the province of Xinjiang, China, were selected as samples. The trees were 27, 29, and 55 years old. The selected disks were from freshly cut trees, and the moisture contents (MC) using the ovendry method were 49.2, 63.5, and 58.3 percent for the 27-, 29-, and 55-year-old trees, respectively. Stress wave velocity was measured in five different experiments with a Fakopp Microsecond Timer to investigate stress wave trends. The following five parts of the experiment were carried out in a laboratory of the Research Institute of Wood Industry, Chinese Academy of Forestry.

1. Three 10-cm-thick disks (diameters, 22.6, 25.7, and 19.6 cm) were cut in half, and three half-disks were selected to be tested by the Fakopp Microsecond Timer at 10° intervals from 0° to 180° (six quarter-disks were used to analyze the results from 0° to 90°). For testing transmission time, the wave source (impacting sensor) was installed at the center of each half-disk, while the receiving sensor was installed at the disk perimeter and moved as each angle changed.
2. Three half-disks were selected as the samples for studying the trend of stress wave transmission in three trees of different ages. For a more accurate determination of change in stress wave velocity with age, the disk from the 27-year-old tree was initially tested on the third annual ring and subsequently tested at an interval of every second annual ring. The same method was used for the disk from the 29-year-old tree, but the initial test was at the seventh annual ring. For the disk from the 55-year-old tree, the initial test was made at the 11th annual ring, and the interval for subsequent tests was four annual rings.
3. Normal wood (two disks) and tension wood (one disk) were used to measure the stress wave velocity, and results were compared for change in velocity. The impacting sensor was located in the pith, and the receiving sensor was successively installed at 1-cm intervals from the pith to the bark.
4. Three totally sound wood disks were used as samples for testing stress wave velocity at 90° and 180° angles between the impacting and receiving sensors. After finishing the first step, a hole was drilled in the center of each disk and progressively enlarged by 1 cm in diameter before each test. A relationship between hole diameter and velocity was established.
5. Simulation of the wavefront of stress waves was conducted on cross sections of disks that were (1) 100 percent sound (sound wood), (2) containing a hole, (3) containing a crack, and (4) containing decay (the decayed disk was an air-dried disk from Inner Mongolia with 7% MC and a thickness of 10 cm). In the cross section, a grid map (1 by 1-cm grid lines) was used to guide the measurement of transmission time from each intersection point to the wave source. The wave source was installed at the north end of the disk, and the receiving sensor was inserted at the grid point at a 45° angle. To provide the same maximum strength signal, a steel ball (2 cm in diameter) from the Metriguard Model 239A Stress Wave Timer, was dropped to always tap the wave source from the same height.

The velocity (v) of stress waves were calculated with the following equation:

$$v = s/t$$

where s is the travel distance of the stress wave in wood and t is the transmission time.

The increase in the ratio of transmission time (IRTT) was calculated as follows:

$$\mathrm{IRTT} = \frac{T_1 - T_2}{T_2} \times 100$$

where T_1 is the transmission time in a disk with a hole and T_2 is the transmission time in a disk without a hole.

Images of stress wave velocity were created by Golden Software Surfer (Version 9.0) to show transmission tracking of stress wave propagation in a cross section of wood.

Results and Discussion

Propagation trend of stress wave in solid wood

Table 1 shows the changes in stress wave velocity as the angle between impacting and receiving sensors was increased from 0° to 90°. Velocity in the radial direction (1,073 m/s) was faster than that in the tangential direction in a cross section of the stem. This is possibly related to the characteristics of P-wave transmission in wood and the microstructure of wood. The actual cause, however, requires further in-depth study.

Figure 1 shows the velocity trend as the angle between sensors changed. An increase in the angle led to a decrease in velocity The ratio of velocity to angle decreased by 1.9 percent when the test angle changed from 0° to 40°. After that, the ratios increased to 9.6, 15.7, 27.0, 49.0, and 78.6 percent when the angle was changed in 10° increments from 50° to 90°, respectively. Statistical analysis showed that velocity was significantly affected by the angle between the impacting and receiving sensors (F value of 19.9, significant at 0.05 level). For the relationship between angle and

Table 1.—Velocity of stress wave based on for different test angles between the transmitting and receiving sensors from 0° to 90°.

Angle (°)	Velocity (m/s)			Coefficient of variation (%)	Precision index (%)
	Maximum	Minimum	Mean ± SD		
0	1,083	1,066	1,073 ± 7.59	0.71	0.58
10	1,101	1,028	1,067 ± 26.78	2.51	2.05
20	1,142	1,032	1,072 ± 38.47	3.59	2.93
30	1,104	968	1,044 ± 49.32	4.73	3.86
40	1,099	970	1,026 ± 43.09	4.20	3.43
50	1,071	891	975 ± 63.92	6.56	5.35
60	994	840	920 ± 53.02	5.76	4.71
70	959	705	825 ± 93.75	11.37	9.28
80	868	283	669 ± 207.98	31.11	25.40
90	805	250	547 ± 194.21	35.50	28.98

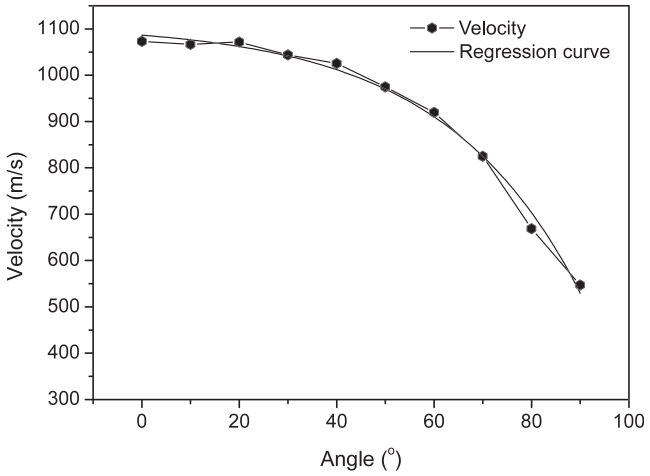

Figure 1.—Trend and regression curve between stress wave velocity and the angle between sensors.

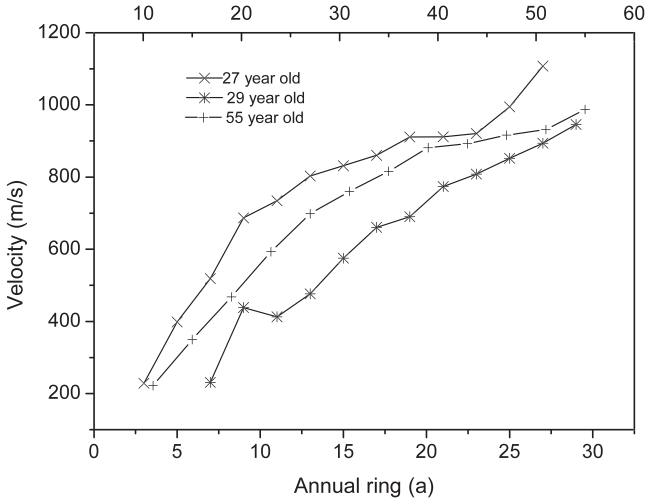

Figure 2.—Stress wave velocity graph for cross sections from 27-, 29-, and 55-year-old trees showing the change in velocity across rings as the transmitting sensor is moved successively from near the pith toward the bark.

velocity, the regression equation is

$$y = -0.984x^2 + 3.2964x + 1,053.7 \quad (r = 0.9961)$$

A departure from this relationship can provide information for assessing internal stem condition in accordance with the change in velocity, especially with respect to the decay of a tree trunk using stress wave tomography.

Figure 2 shows the trends of velocity in 27-, 29-, and 55-year-old wood specimens, with each curve representing the velocity variation for different annual ring intervals. All velocities increased as annual rings increased, with velocity ranging from 228 to 1,107, from 231 to 945, and from 133 to 968 m/s, respectively, for the three specimens. A lower velocity was found near the pith, where stress wave transmittance was affected by the structure of the early (i.e., juvenile) wood (i.e., low density and stiffness). Velocity gradually increased as the percentage of mature wood increased, but the increasing ratio of velocity to angle caused a slightly flatter slope for the curves when mature wood become the main component in the cross section.

Figure 3 plots the variation in velocity from pith to bark in Euphrates poplar for both normal and tension wood**.** For both types of wood, velocity showed a gradual increase as the radial distance increased. The velocity ranged from 353 to 1,111 m/s in normal wood and from 278 to 997 m/s in tension wood. A detailed examination of the curves shows that the tension wood exhibited slightly lower velocities

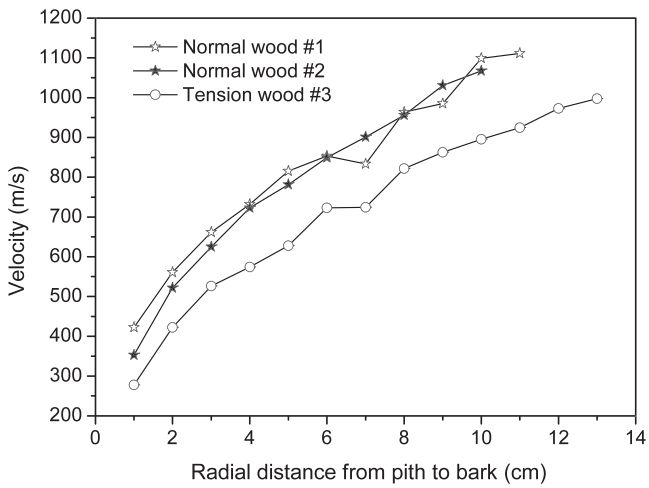

Figure 3.—Sound velocity as a function of distance from pith to bark in cross sections of normal wood and tension wood.

compared with normal wood. Fibers are the basic anatomical element for wave propagation, and in tension wood, fibers are longer than in normal wood. Fibers in tension wood also have lower lignin content, and the fiber and

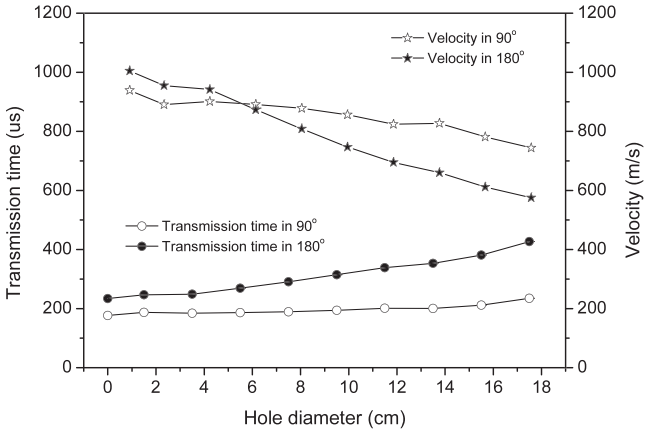

Figure 4.—Slope of transmission time and velocity of stress waves encountering different hole diameters at 90° and 180° angles.

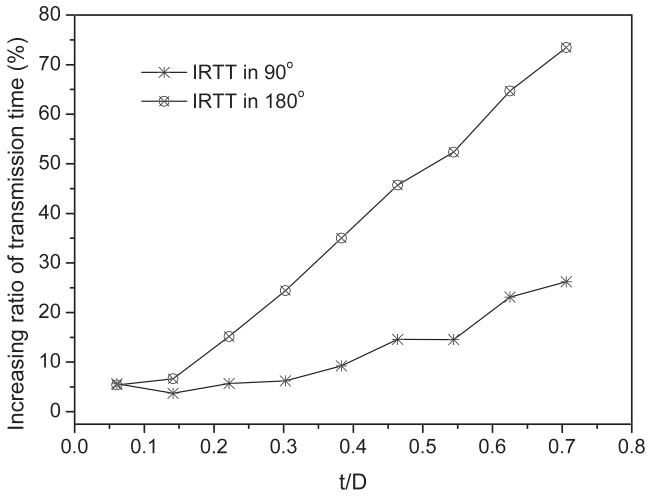

Figure 5.—Slope of transmission time for increasing t/D *with transducer angles of 90° and 180°.*

vessel area of a tension wood cross section is lower in the radial direction than that of a normal wood cross section.

Propagation trend of stress waves in a cross section containing a hole

Figure 4 shows transmission time and velocity of stress waves through a cross section of wood in which artificial holes, ranging in diameter from 1.5 to 17.5 cm, have been introduced. The holes caused a slight increase in transmission time at the 90° angle between impacting and receiving sensors. The change was minimal, however, because the stress wave path was not through the center of the disk. The propagation path traversed through the sound wood when the radius of the hole was less than the vertical distance from the center of the hole to the propagation path. However, transmission time for the 180° angle was affected by the diameter of the hole. When holes were made in sound wood, a clear decrease in stress wave velocity was found at the 180° angle compared with that of sound wood without holes. Furthermore, the larger the hole, the more the velocity decreased. Statistical analysis showed a linear relationship between hole diameter and transmission time (positive relationship) and between hole diameter and velocity (negative relationship; Table 2).

To avoid having the individual property differences of the disks influence the IRTT, the hole/disk diameter (t/D) value was used to analyze the time change at the 90° and 180° angles. The IRTT in the 90° angle was less than 10 percent when t/D equaled 0.38 and increased to 26.2 percent when the t/D was 0.71. For the 180° angle, the IRTT was 35 and 73.5 percent, respectively. Figure 5 shows that although the slope of the transmission time for the 90° angle between transducers was positive, it was not as steep as that for the 180° angle when the t/D was 0.22. Calculations for the IRTT, for both angles, initially had a negative slope when t/D increased, but the slope became positive when t/D equaled 0.25. These data relationships can be used to assess internal decay or holes in tree stems, because they are not be affected by the individual properties of trees, temperature, or MC.

Simulating wavefronts of stress waves in cross section of wood

The wavefronts of stress waves in a cross section of wood were depicted by measuring the contour of the transmission time to simulate a stress wave path over a time duration as the wave passed through sound, hole, crack, and decay wood. Figure 6 depicts a wavefront in sound wood in which the stress wave spreads out from the initiation point and shows that the radial direction has the fastest transmission compared with other directions. From the radial to tangential direction, the wavefront gradually narrows. If the wave passed the pith, however, it was blocked because of the low density of the wood, leading to increased wave impedance and increased transmission time, especially in the radial direction. Beyond the pith, transmission time in other directions is faster than in the radial direction (Fig. 6a).

For cross sections with cracks, the vibration path was more complex and interrupted than for sound wood, although the configuration of the wavefront was similar to

Table 2.—Regression analysis of stress wave transmission time and velocity for different hole diameters.[a]

Angle (°)	Linear regression ($y = a + bx$)					Critical value, $r_{0.01} = (n - 2)$
	y	x	a	b	r	
90	Transmission time (μs)	Hole diameter (cm)	168.83	5.0256	0.9042	0.7646
	Velocity (m/s)	Hole diameter (cm)	956.51	−18.80	0.9619	0.7646
180	Transmission time (μs)	Hole diameter (cm)	195.93	20.799	0.9822	0.7646
	Velocity (m/s)	Hole diameter (cm)	1,062.8	−50.133	0.9956	0.7646

[a] All results are significant at the 0.05 level.

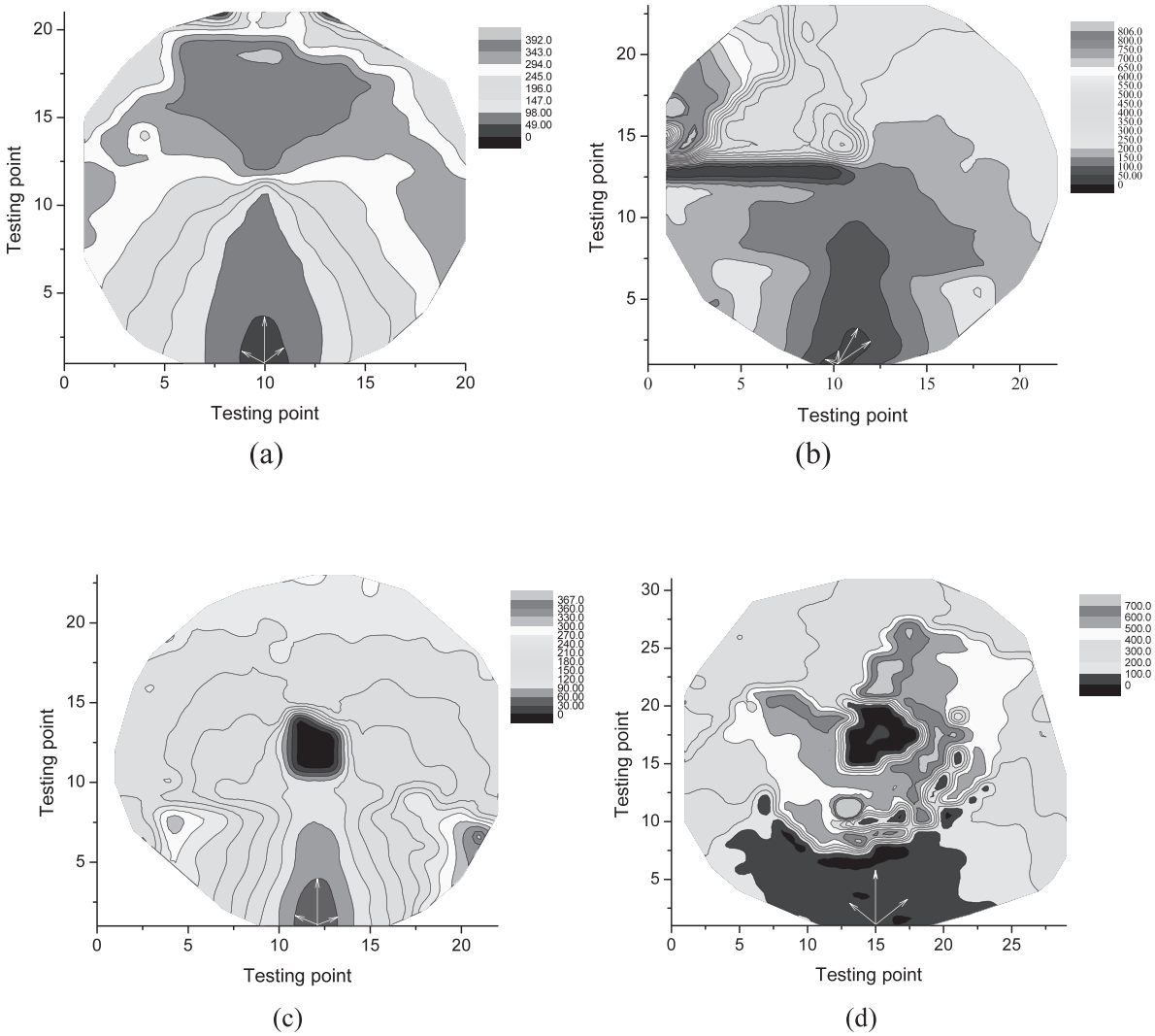

Figure 6.—Two-dimensional maps of wavefronts from transmission time of stress waves in cross section of wood: (a) sound wood, (b) wood with manually induced crack, (c) wood with manually induced hole, and (d) wood with decay.

that for sound wood at the initiation point, with the radial direction still the fastest when located in the beginning of the path (Fig. 6b). However, the transmission time was lengthened when the wave encountered a crack and the path changed to go around the crack. The wavefront shows the position and dimension of the crack, but more studies of stress wave tomography are needed to provide an accurate assessment of crack properties in a stem.

In the cross section with a hole, the wavefront showed good configuration in the sound wood before the stress wave path encountered the hole (Fig. 6c). After passing the hole, the stress wave was affected such that the transmission time increased as the path had to move around the hole, and the configuration of the wavefront appeared to have a callback pattern.

The wavefront did not show a good path in severely decayed wood as the stress wave lost direction. The loss of direction was greatest in severely decayed wood compared with sound wood and lightly decayed wood. Decay affected the transmission of the stress wave so that the wavefront could not produce a path with consistent results (Fig. 6d).

Figure 7 shows simulated 3D maps made with Golden Software Surfer (Version 9.0) based on the velocity of stress waves mapped on a 1 by 1-cm grid. Kriging interpolation enables us to increase the value of velocity and both accurately simulate the map and show more information in a cross section. High velocity formed high points in the grid, but the surface would then drop down after passing through the pith in sound wood (Fig. 7a). A crack was also manually simulated in the map, but the width was less when compared with the real disk. The main reason for this was that after interpolation, the velocity value of the simulation was greater than both the test value and the velocity at the edge of the crack in sound wood. The high velocity partially offset the grid velocity from the crack, which led to the decrease in the dimension of the crack (Fig. 7b). For the map representing the hole in the cross section of the wood, the dimension and shape of the hole were presented in the center of the map by the high grid surface. Except for the hole position, all cross sections were sound wood (Fig. 7c). In the map showing severe decay, however, low velocity was shown by the grid surface being lower than in the other maps (Fig. 7d).

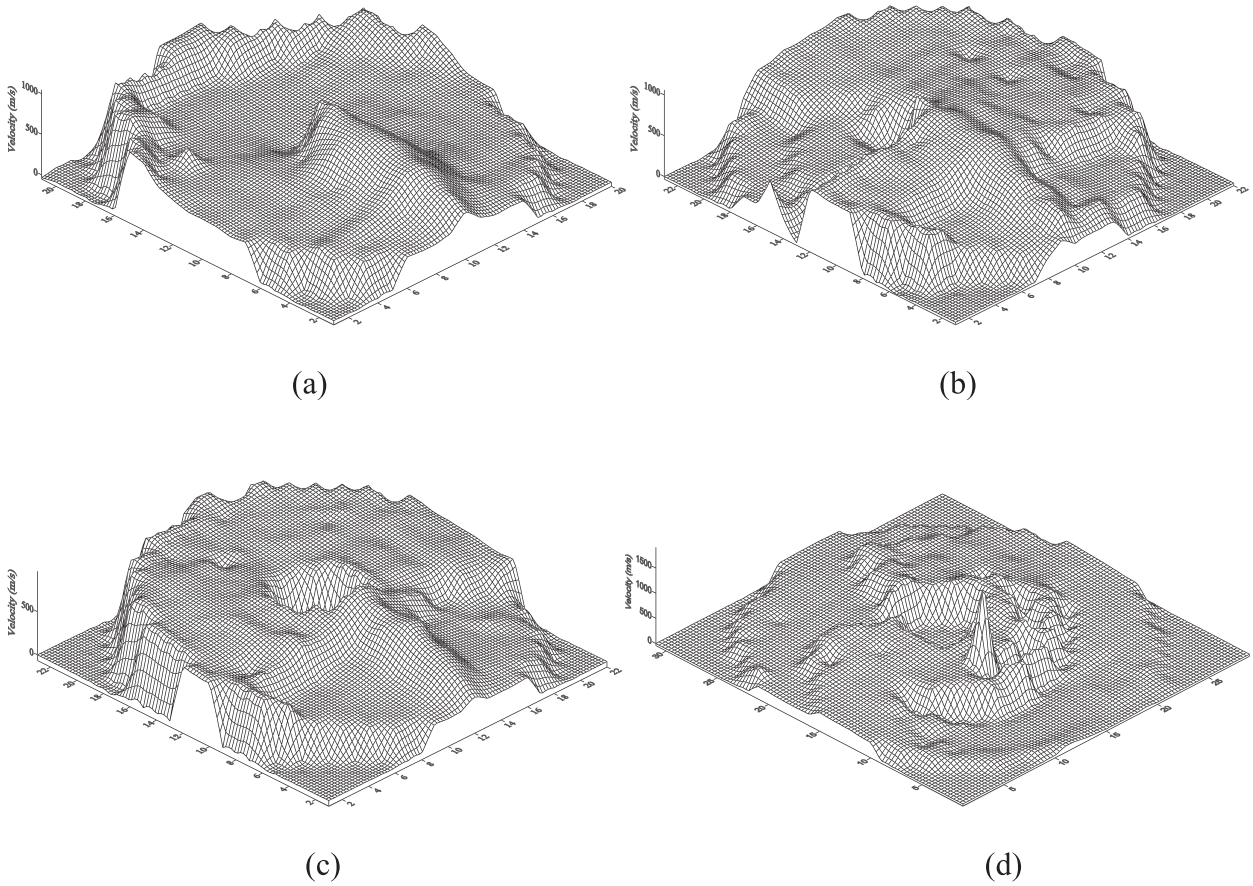

Figure 7.—Three-dimensional maps of wavefronts from velocity of stress waves in cross sections of wood: (a) sound wood, (b) wood with crack, (c) wood with hole, and (d) wood with decay.

The wavefront simulation maps show the paths of stress waves in sound, crack, hole, and decay wood. Of course, in-depth examination of the wavefront patterns of the stress waves is also needed for many other types of defects in wood. These other defects (and combinations of defects) will require more involved simulation processes. The results of the current study are intended to present a method of simulating stress wave paths in the cross section of a tree stem, to further our understanding of stress wave transmission paths, and to provide more information for use in detecting defects in wood.

Summary and Conclusion

Controlled experiments to examine stress wave variations in tree stem cross sections were performed. Results indicated that velocity gradually decreased when the test angle changed from a radial direction to a tangential direction. An increase in velocity occurred with an increase in annual rings and an increase in radial distance from pith to bark in normal wood and in tension wood; however, the velocity in normal wood was higher than that in tension wood. Furthermore, a hole in the center of a cross section produced little change in velocity when the hole increased in diameter given a 90° angle between the impacting and receiving sensors. At 180°, however, the velocity rapidly decreased with the increase in hole diameter. The wavefronts of stress waves through cross sections of sound, hole, crack, or decay wood were successfully simulated and presented by contour maps. Furthermore, 3D maps of velocity were constructed through Kriging interpolation to present the real structure of a tree stem cross section.

Acknowledgments

This study was supported by the Wood-Inorganic Restoration Material Project from Technique Introduction and Innovation of Bio-Macromolecule New Material of Introducing Overseas Advanced Forest Technology Important Program of China (2006-4-C03). We are grateful for and acknowledge the financial support. We also greatly appreciate Mr. James H. Muehl for his comprehensive review and suggestions for enhancing this paper.

Literature Cited

Divos, F. and P. Divos. 2005. Resolution of stress wave based acoustic tomography. *In:* Proceedings of the 14th International Symposium on Nondestructive Testing of Wood, May 2–4, 2005, University of Applied Sciences, Eberswalde, Germany; Shaker Verlag, Eberswalde, Germany. pp. 309–314.

Divos, F. and L. Sazlai. 2002. Tree evaluation by acoustic tomography. *In:* Proceedings of the 13th International Symposium on Nondestructive Testing of Wood, August 19–21, 2002, Berkeley, California. pp. 251–256.

Gilbert, E. A. and E. T. Smiley. 2004. Picus sonic tomography for the quantification of decay in white oak (*Quercus albea*) and hickory (*Carya* spp.). *J. Arboric*. 30(5):277–280.

Grabianowski, M., B. Manley, and J. C. F. Walker. 2006. Acoustic measurements on standing trees, logs and green lumber. *Wood Sci. Technol*. 40:205–216.

Larsson, B., B. Bengtsson, and M. Gustafsson. 2004. Nondestructive detection of decay in living trees. *Tree Physiol*. 24:853–858.

Liang, S., X. Wang, Z. Cai, J. R. Ross, and F. Fu. 2008. Elastic wave tomography in standing tree decay detection. *Sci. Silvae Sin*. 44(5): 109–114. (In Chinese.)

Nicolotti, G., L. V. Socco, R. Martinis, A. Godio, and L. Smabuelli. 2003. Application and comparison of three tomographic techniques for detection of decay in trees. *J. Arboric*. 29(2):66–78.

Pellerin, R. F., R. C. Degroot, and G. R. Esenther. 1986. Nondestructive stress wave measurements of decay and termite attack in experimental wood units. *In:* Proceedings of the Fifth Nondestructive Testing of Wood Symposium, September 9–11, 1985, Washington State University, Pullman; Washington State University, Pullman. pp. 315–352.

Ross, J. R., R. F. Pellerin, N. Volny, W. W. Salsig, and R. H. Falk. 1999. Inspection of timber bridges using stress wave timing nondestructive evaluation tools—A guide for use and interpretation. General Technical Report FPL-GTR-114. http://www.fpl.fs.fed.us/documnts/fplgtr/fplgtr114.pdf. Accessed December 20, 2008.

Ross, J. R., C. J. Ward, and A. TenWolde. 1994. Identifying bacterially infected oak by stress wave nondestructive evaluation. Research Paper FPL-RP-512. http://www.fpl.fs.fed.us/documnts/fplrp/fplrp512.pdf. Accessed July 5, 2008.

Schad, C. K., L. D. Schmoldt, and J. R. Ross. 1996. Nondestructive methods for detecting defects in softwood logs. Research Paper FPL-RP-546. http://www.fpl.fs.fed.us/documnts/fplrp/fplrp546.pdf. Accessed October 17, 2008.

Schwarze, F. W. M. R., C. Rabe, D. Ferner, and S. Fink. 2004. Detection of decay in trees with stress waves and interpretation of acoustic tomograms. *J. Arboric*. 28(1):3–19.

Wang, L., H. Xu, C. Zhou, L. Li, and X. Yang. 2007. Effect of sensor quantity on measurement accuracy of log inner defects by using stress wave. *J. Forestry Res*. 18(3):221–225.

Wang, X., F. Divos, C. Pilon, B. K. Brashaw, R. J. Ross, and R. F. Pellerin. 2004. Assessment of decay in standing timber using stress wave timing nondestructive evaluation tools—A guide for use and interpretation. General Technical Report FPL-GTR-147. http://www.fpl.fs.fed.us/documnts/fplgtr/fpl_gtr147.pdf. Accessed February 23, 2009.

Wang, X., J. R. Ross, and P. Carter. 2005a. Acoustic evaluation of standing trees-resent research development. *In:* Proceedings of the 14th International Symposium on Nondestructive Testing of Wood, May 2–4, 2005, University of Applied Sciences, Eberswalde, Germany; Shaker Verlag, Eberswalde, Germany. pp. 455–465.

Wang, X., J. Wiedenbeck, and S. Liang. 2009. Acoustic tomography for decay detection in black cherry tress. *Wood Fiber Sci*. 41(2):1–11.

Wang, X., J. Wiedenbeck, J. R. Ross, J. W. Forsman, J. R. Erickson, C. Pilon, and B. K. Brashaw. 2005b. Nondestructive evaluation of incipient decay in hardwood logs. General Technical Report FPL-GTR-162. http://www.fpl.fs.fed.us/documnts/fplgtr/fpl_gtr162.pdf. Accessed March 16, 2009.

Yamamoto, K., O. Sulaiman, and R. Hashim. 1998. Nondestructive detection of heart rot of acacia mangium trees in Malaysia. *Forest Prod. J*. (3):83–86.